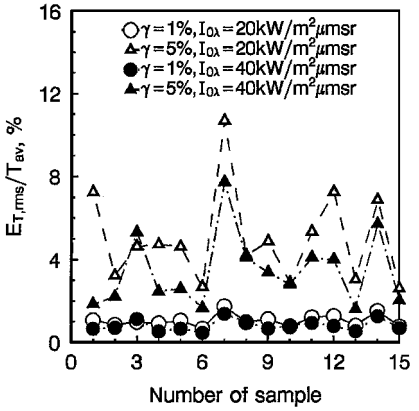

Fig. 3 Errors of estimation of temperature using noisy input data.

coefficient is more sensitive to the measurement errors. By comparing the results of the cases of $I_{0\lambda} = 20$ and 40 kW/m^2 μmsr, it can clearly be seen that increasing the spectral radiative intensity of the laser can improve the accuracy of the reconstruction of absorption coefficient because the accuracy of measured transmittance defined by Eq. (4) will be improved by increasing the spectral radiative intensity of the laser.

For all cases just considered, calculations are started with an initial guesses $\boldsymbol{a}$ and $\boldsymbol{b} = 0$. The CPU time required for each sample of estimation calculation varied from 10 s to 1 min on a personal computer with a 450 MHz Pentium III processor.

Conclusions

An inverse analysis is presented for the estimation of temperature and absorption coefficient profiles for an axisymmetric free flame from the knowledge of the out going spectral emission and transmission radiation intensities. The source term and absorption coefficient profiles are expressed as polynomial-type functions of space ordinate. The inverse problem is formulated in terms of two optimization problems, and the conjugate gradient method is used. Although the temperature and the absorption coefficient are the functions of space variable, the inverse algorithm presented requires measurements of the outgoing radiative intensities only at several different positions of the line of sight. Both exact and noisy input data have been used to test the performance of the proposed method. The effects of measurement errors on the accuracy of the estimations are examined. The results show that the profiles of temperature can be estimated accurately, even with noisy data, but the absorption coefficient is more sensitive to the measurement errors. Increasing the radiative intensity of the laser can improve the accuracy of the absorption coefficient reconstruction.

Acknowledgments

We gratefully acknowledge the National Science Foundation of China, the Chinese National Science Fund for Distinguished Young Scholars, and the Science Fund of the Harbin Institute of Technology for supporting this work.

References

[1]Zhang, J. Q., and Cheng, J. S., "Determination of the Temperature Profile of Axisymmetric Combustion-Gas Flow from Infrared Spectral Measurements," *Combustion and Flame*, Vol. 65, No. 2, 1986, pp. 163–176.

[2]Yousefian, Y., and Lallemand, M., "Inverse Radiative Analysis of High-Resolution Infrared Emission Data for Temperature and Species Profiles Recoveries in Axisymmetric Semitransparent Media," *Journal of Quantitative Spectroscopy and Radiative Transfer*, Vol. 60, No. 6, 1998, pp. 921–931.

[3]Yousefian, Y., Sakami, M., and Lallemand, M., "Recovery of Temperature and Species Concentration Profiles in Flames Using Low-Resolution Infrared Spectroscopy," *Journal of Heat Transfer*, Vol. 121, No. 2, 1999, pp. 268–279.

[4]Solomon, P. R., Best, P. E., Carangelo, R. M., Markham, J. R., and Chien, P. L., "FT-IR Emission/Transmission Spectroscopy for In Situ Combustion Diagnostics," *Proceedings of the Twenty-First International Symposium on Combustion*, Combustion Inst., Pittsburgh, PA, 1986, pp. 1763–1771.

[5]Best, P. E., Chien, P. L., Carangelo, R. M., Solomon, P. R., Danchak, M., and Ilovici, I., "Tomographic Reconstruction of FT-IR Emission and Transmission Spectra in a Sooting Laminar Diffusion Flame: Species Concentration and Temperatures," *Combustion and Flame*, Vol. 85, No. 3, 1991, pp. 309–318.

[6]Hall, R. J., and Bonczyk, P. A., "Sooting Flame Thermometry Using Emission/Absorption Tomography," *Applied Optics*, Vol. 29, No. 31, 1990, pp. 4590–4598.

[7]Li, H. Y., and Ozisik, M. N., "Identification of the Temperature Profile in an Absorbing, Emitting, and Isotropically Scattering Medium by Inverse Analysis," *Journal of Heat Transfer*, Vol. 114, No. 4, 1992, pp. 1060–1063.

[8]Siewert, C. E., "An Inverse Source Problem in Radiative Transfer," *Journal of Quantitative Spectroscopy and Radiative Transfer*, Vol. 50, No. 6, 1993, pp. 603–609.

[9]Siewert, C. E., "A Radiative-Transfer Inverse-Source Problem for a Sphere," *Journal of Quantitative Spectroscopy and Radiative Transfer*, Vol. 52, No. 2, 1994, pp. 157–160.

[10]Li, H. Y., "Estimation of the Temperature Profile in a Cylindrical Medium by Inverse Analysis," *Journal of Quantitative Spectroscopy and Radiative Transfer*, Vol. 52, No. 6, 1994, pp. 755–764.

Mass-Flux and Shock Calculations Through Cryogenic Homogeneous Two-Phase Nozzle Flow

I. Sinan Akmandor*
Middle East Technical University, 06531 Ankara, Turkey
and
Toshio Nagashima†
University of Tokyo, Tokyo 113-8656, Japan

Nomenclature

$A(\xi)$	= nozzle cross-sectional area
C	= mixture specific heat constant
K	= $1 + R_G X/C$, parameter replacing γ in homogeneous two-phase flow
$\dot{m}$	= mass-flow rate
N	= linearity parameter in the Henry–Fauske flow quality derivative[l]
p	= pressure
R_G	= vapor-phase gas constant
T	= local mixture temperature
X	= flow quality
α	= void fraction
γ	= vapor-phase specific heat ratio
v	= specific volume
ξ	= axial distance
ρ	= mixture density

Subscripts

e	= equilibrium
G	= vapor phase
L	= liquid phase
t	= total quantity
th	= throat location
1	= upstream of shock
2	= downstream of shock

Presented as Paper 99-0347 at the AIAA 37th Aerospace Sciences Meeting, Reno, NV, 11–14 January 1999; received 5 August 1999; revision received 5 February 2000; accepted for publication 28 February 2000.

*Associate Professor, Department of Aeronautical Engineering.
†Professor, Department of Aeronautics and Astronautics, Bunkyo-ku.

I. Introduction

A SIMPLE convergent-divergentnozzle geometry is used to analyze the steady shock wave front of the two-phase, subcooled nitrogen flow, which is initially almost liquid.[1] The vapor phase is supposed to be uniformly distributed so that the medium is approximately homogeneous. A two-phase Newton–Raphson implicit Euler scheme is used in the numerical simulation. Some results of the present algorithm have already been extensively compared with our previous results due to an implicit unsteady total variation-diminishing scheme.[2]

II. Analytical Mass-Flux Models

Henry–Fauske analytic mass flux model[3] has been derived in detail in the work of Simoneau and Hendricks.[1] The choked throat mass flux is given by

$$\frac{\dot{m}}{A(\xi)} = -\left(X\frac{\mathrm{d}v_G}{\mathrm{d}p} + (v_G - v_L)N\frac{\mathrm{d}X_e}{\mathrm{d}p}\right)^{-\frac{1}{2}}_{\text{th}} \tag{1}$$

A second analytical mass flux expression[2] has also been used:

$$\frac{\dot{m}}{A(\xi)} = \frac{P_t}{\sqrt{T_t}}\sqrt{\frac{K}{R_G X}}M \times\left(1 + \frac{K-1}{2}\frac{K/\alpha}{\alpha + K - 1}M^2\right)^{-(\gamma+1)/2(\gamma-1)} \tag{2}$$

The power of this equation has been empirically modified from $(K+1)/2(K-1)$ to $(\gamma+1)/2(\gamma-1)$ to avoid unrealistically large power magnitudes. This also ensures that the local pressure is mainly dictated by the vapor phase.

III. Two-Phase Shock-Jump Relations

The two-phase shock-jump relations are derived from the one-dimensional conservation equations. The quality X is assumed to be constant:

$$\frac{p_2}{p_1} = \frac{\left[1 + K\left(M_1^2 |\ \alpha_1\right)\right]}{\left[1 + K\left(M_2^2 |\ \alpha_2\right)\right]} \tag{3}$$

$$\alpha_2 = 1 - (1-\alpha_1)\left(\frac{M_1^2}{\alpha_1}\right)\left(\frac{\alpha_2}{M_2^2}\right)\frac{\left[1 + K\left(M_2^2 |\ \alpha_2\right)\right]}{\left[1 + K\left(M_1^2 |\ \alpha_1\right)\right]} \tag{4}$$

Table 1 Experimental, analytical, and numerical mass flux

Run	Inlet Pt, Mpa	Back pressure, Mpa	Saturation pressure, Mpa	Experimental mass flux, kg/m^2 · s	Modified analytical mass flux, kg/m^2 · s	Henry–Fauske mass flux, kg/m^2 · s	Numerical mass flux, kg/m^2 · s	Inlet void
101-863	2.41	0.57	1.49	36,600	37,259.70	34,416.57	36,641.95	0.1
101-874	2.51	0.36	1.45	37,800	37,433.94	34,621.38	37,601.96	0.1
101-457	2.65	0.51	1.51	38,800	43,853.82	39,152.77	38,828.34	0.06
101-868	2.83	0.38	1.46	41,700	44,292.98	40,326.35	41,740.18	0.06
101-889	3.07	0.64	1.45	45,300	48,451.42	44,981.08	45,300	0.045
101-476	3.19	0.76	1.46	46,300	49,231.75	45,020.57	46,300.01	0.045
101-902	3.36	0.93	1.5	48,000	51,320.13	46,434.8	48,033.02	0.04
101-881	3.67	0.84	1.5	51,800	52,242.58	47,011.43	51,840.82	0.04
101-907	3.9	0.65	1.51	54,000	54,080.78	48,375.37	54,047.16	0.04
101-910	4.26	0.5	1.47	58,200	62,548.02	53,146.75	58,238.77	0.02
101-921	4.72	0.86	1.47	62,500	64,507.69	53,369	62,537.71	0.02
101-895	5.2	1.01	1.46	67,100	64,662.38	54,762.88	66,999	0.02
101-914	5.43	0.56	1.47	69,100	69,234.64	56,813.92	69,157.37	0.015
101-474	6.17	0.74	1.5	75,100	78,771.85	67,266.53	75,099.99	0.01
101-918	6.45	0.61	1.46	77,100	79,847.37	66,761.03	77,151.37	0.01
101-460	6.64	0.4	1.46	78,900	83,086.57	72,475.15	78,940.84	0.0075

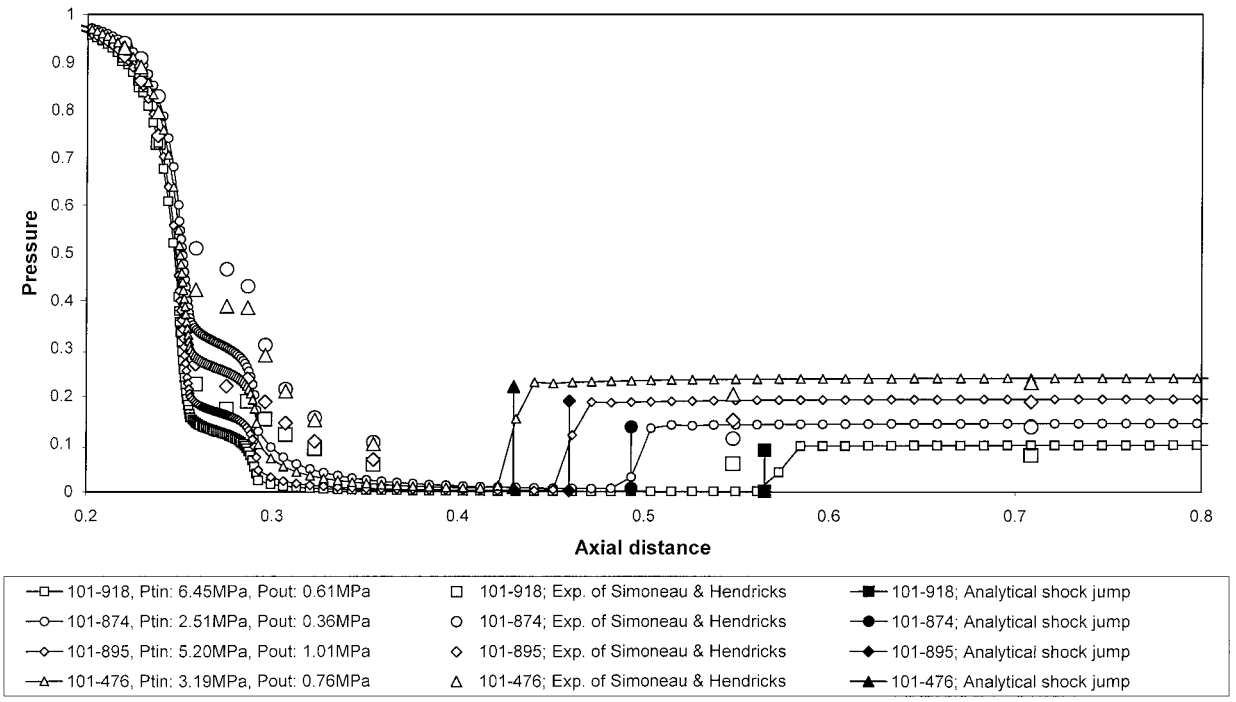

Fig. 1 Axial pressure profiles.

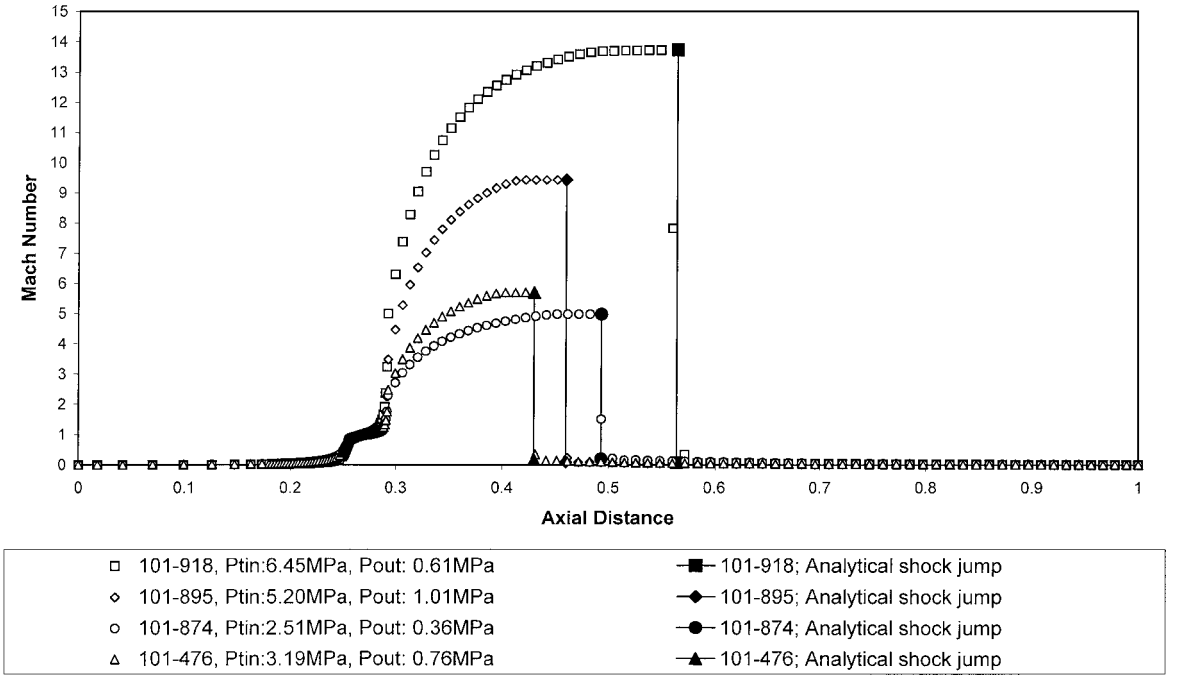

Fig. 2 Axial Mach-number profiles.

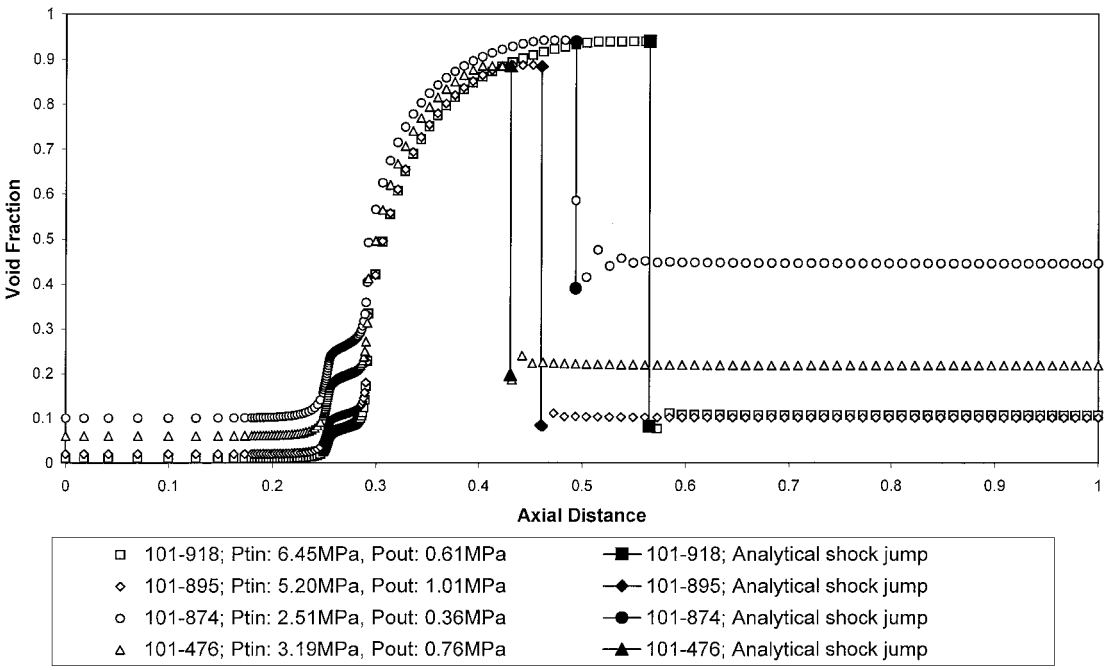

Fig. 3 Axial void fraction profiles.

These equations lead to a single shock-jump expression where the unknown is (M_2^2/α_2):

$$\frac{\{1+[\alpha_1/(K-1)]+(K/2)(M_1^2|\ \alpha_1)\}(M_1^2|\ \alpha_1)}{[1+K(M_1^2|\ \alpha_1)]^2}$$

$$\times[1+K(M_2^2|\ \alpha_2)]^2=\frac{K}{2}\left(\frac{M_2^2}{\alpha_2}\right)^2+\left(1+\frac{1}{K-1}\right)\left(\frac{M_2^2}{\alpha_2}\right)$$

$$-\left\{\frac{1-\alpha_1}{K-1}\frac{(M_1^2|\ \alpha_1)}{[1+K(M_1^2|\ \alpha_1)]}\right\}[1+K(M_2^2|\ \alpha_2)] \qquad (5)$$

Given upstream values for K, M_1, α_1, this equation is solved, and the remaining dependent variables p_2/p_1, M_2, and α_2 are found by backsubstituting M_2^2/α_2.

IV. Results and Discussion

The nozzle geometry of Simoneau and Hendricks has been used. The convergent section slope angle is 6.79 deg, and the inlet area is 3.896 cm^2. The divergent section slope angle is 3.78 deg, and the exit area is 8.360 cm^2. The choked throat area is 0.09926 cm^2. The experimental data series (101-863)–(101-460) has a wide range of inlet-to-exit nozzle pressure ratio, and the corresponding analytical and numerical mass fluxes have been calculated. The inlet total temperature is around 110 K.

The inlet void fractions, which have been used as numerical boundary conditions, are also given in Table 1. The analytical Henry–Fauske mass-flux model seems to agree less for high inlet pressures. The axial pressure profiles are presented in Fig. 1, along with experimental and analytical shock-jump values. The pressure values have been nondimensionalized with respect to the inlet stagnation pressure. Although, there are not enough experimental data

in the shock location, there is agreement between numerical and analytical pressure jumps. Figure 2 is the axial distribution of Mach-number profiles, where the agreement between the numerical and analytical shock jump is apparent. The effect of the sharp expansion corner after the flat nozzle throat is reflected in the Mach-number profiles. Figure 3 is the numerical void fraction profiles. Despite the wide range of pressure ratio and inlet void fractions among the four runs, there is again agreement between numerical and analytical shock jumps.

V. Conclusion

Numerical mass-flux results have been compared to experimental and analytical mass-flux values. The amount of inlet void fraction, together with inlet total pressure and temperature, sets the mass-flux level. Analytic and numerical shock jumps of pressure, Mach number, and void are in close agreement.

References

[1]Simoneau, R. J., and Hendricks, R. C., "Two-Phase Choked Flow of Cryogenic Fluids in Converging-Diverging Nozzles," NASA TP 1484, July 1979.

[2]Akmandor, I. S., and Nagashima, T., "Predictions for Cryogenic Homogeneous Two-Phase Flows in Choked Laval Nozzles," *Journal of Thermophysics and Heat Transfer,* Vol. 13, No. 3, 1999, pp. 355–363.

[3]Henry, R. E., and Fauske, H. K., "The Two-Phase Critical Flow of One-Component Mixtures in Nozzles, Orifices and Short Tubes," *Journal of Heat Transfer,* Vol. 93, Series C, No. 2, 1971, pp. 179–187.

Influence of $O_2(v) + N = NO + O$ on NO Formation in One-Dimensional Air Nozzle Flow

G. Colonna,* M. Tuttafesta,* and M. Capitelli†
University of Bari, 70126 Bari, Italy
and
D. Giordano‡
ESA, 2200 AG Noordwijk, The Netherlands

In a recent investigation[1,2] we have studied the nonequilibrium state-to-state air vibrational kinetics of air mixtures in one-dimensional nozzle expansion. The main result of this investigation was the strong non-Arrhenius behavior of the NO formation rate through the reaction between vibrationally excited molecules $[N_2(v)]$ and atomic oxygen:

$$N_2(v) + O \leftrightarrow NO + N \quad (1)$$

In turn this was caused by the preferential pumping of high energy levels of nitrogen by the gas-phase recombination reaction generating non-Boltzmann vibrational distributions along the axis of the nozzle. In this Note we present results relative to a further study of the same nozzle expansion. In particular we have inserted the reaction between vibrationally excited O_2 molecules and atomic nitrogen, i.e., the process

$$O_2(v) + N \leftrightarrow NO + O \quad (2)$$

Received 13 August 1999; revision received 23 December 1999; accepted for publication 1 March 2000.

*Researcher, Department of Chemistry, Centro Studi per la Chimica dei Plasmi, Consiglio Nazionale delle Ricerche, Via Orabona 4.

†Full Professor, Department of Chemistry, Centro Studi per la Chimica dei Plasmi, Consiglio Nazionale delle Ricerche, Via Orabona 4.

‡Researcher, Aerothermodynamics Section, European Space Research and Technology Center.

with the double intent to detect any variation of the NO formation rate as well as to understand better the kinetics of O_2/O components in the air mixture.

Process 2 is then inserted in the state-to-state vibrational kinetics reported in Refs. 1 and 2, which in turn is coupled to the fluid dynamics equations describing nozzle expansion. We use the same nozzle geometries (parabolic and F4 nozzle) discussed in Refs. 1 and 2, whereas the state-to-state rate coefficients are those discussed in Refs. 3 and 4.

Complete results of this study have been reported in Ref. 5. In this Note we want to emphasize the differences in the relevant results that occur after introduction of reaction 2.

The calculations performed for a 1-m-long parabolic nozzle (see Fig. 1 of Ref. 1) with reservoir pressure P_0 of about 1 atm and

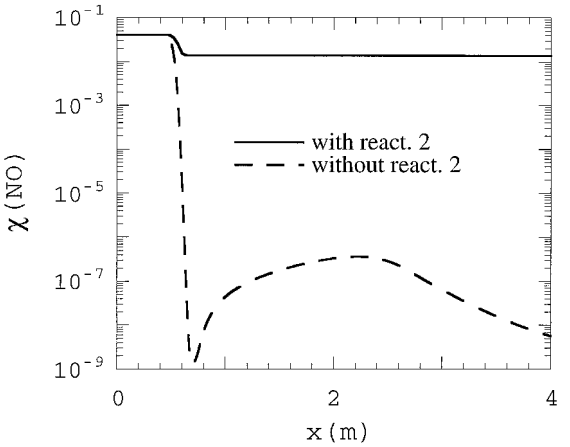

Fig. 1 NO molar fraction profile in F4 nozzle calculated with and without reaction 2.

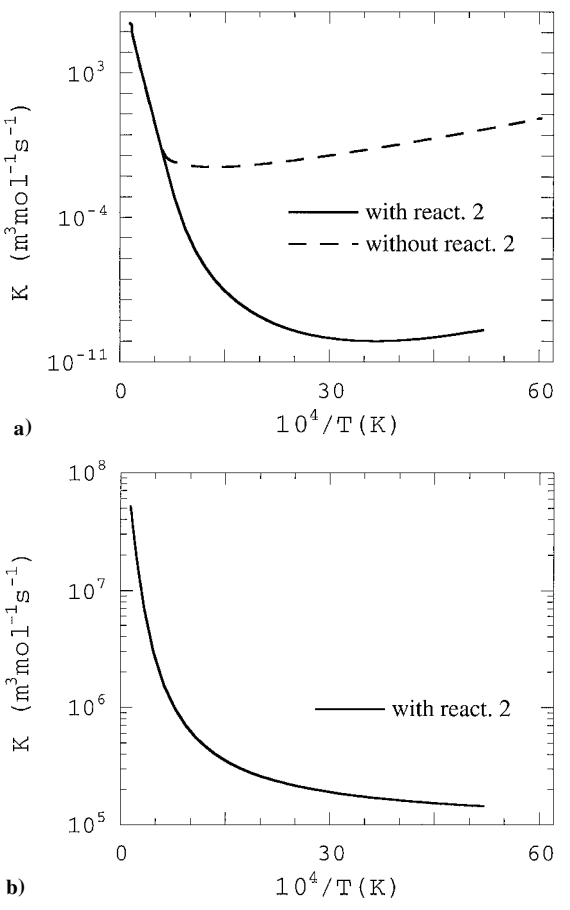

Fig. 2 Arrhenius plot of NO formation rates by a) reaction 1 and b) reaction 2 in F4 nozzle.